Materials Research. 2025; 28:e20240592
DOI: https://doi.org/10.1590/1980-5373-MR-2024-0592

The Impact of Mn^{2+} ions Concentration on Co-electrowinning Using a Dimensionally Stable Anode (Ti/RuO_2): Effects on Physical and Chemical Properties

***Danielle Costal de Castro*[a]*, *Iranildes Daniel dos Santos*[b], *Reiner Neumann*[c], *Pedro Paulo Medeiros Ribeiro*[a], *Achilles Junqueira Bourdot Dutra*[a]**

[a]*Universidade Federal do Rio de Janeiro, Programa de Pós-Graduação em Engenharia Metalúrgica e de Materiais, Rio de Janeiro, RJ, Brasil.*
[b]*Instituto Tecnológico Vale, Ouro Preto, MG, Brasil.*
[c]*Centro de Tecnologia Mineral, Rio de Janeiro, RJ, Brasil.*

Received: December 19, 2024; Revised: March 10, 2025; Accepted: April 02, 2025

Metallic cobalt is valued for its thermal and corrosion resistance. In 2018, cobalt prices surged to 95,250 USD/t, fueled by the growing electric vehicle market. However, metallurgical challenges persist, including cost reduction and impurity control. Manganese, a frequent impurity in cobalt electrowinning from laterite and copper ores, can reach up to 560.6 $mg \cdot L^{-1}$ in leach solutions. Though solvent extraction removes ~90% of manganese, residual amounts impact current efficiency (CE), specific energy consumption (SEC), and deposit quality. Electrowinning tests at 200 $A \cdot m^{-2}$, 60°C, and pH 4 showed that 0.12 $g \cdot L^{-1}$ Mn^{2+} increased CE to 92.2% but raised SEC to 1.96 $kWh \cdot kg^{-1}$. Mn^{2+} altered deposit morphology, reducing microhardness and increasing brittleness. Thermogravimetric analysis revealed ~1.35% mass loss in deposits with Mn^{2+}, while higher concentrations enhanced residual strain and enlarged crystallite sizes. Deposits exhibited primarily hexagonal close-packed (HCP) structures with occasional face-centered cubic (FCC) phases.

Keywords: *Impurity, metallic cobalt, electrowinning, cobalt deposits, manganese ions.*

1. Introduction

Cobalt holds significant strategic importance, with its supply closely tied to the global markets for nickel and copper, as it is predominantly recovered as a byproduct of their extraction processes. Most of the cobalt production comes from copper extraction, followed by the extraction of copper-nickel sulfide and nickel ores[1,2]. The Democratic Republic of Congo (DRC), particularly the Kinshasa region, contains the largest world reserves of cobalt, contributing about 60% of its production. Additional sources of cobalt include copper-nickel sulfide and nickel ores, which account for approximately 23% and 15% of global cobalt extraction, respectively[1-4]. As cobalt is a byproduct of mining, the investigation of the presence of impurities during its extraction is crucial to producing a pure metal deposit with industrially acceptable physical and chemical properties.

Guimarães et al.[5] reported the impurities concentration present in a pregnant leach solution obtained from lateritic nickel ores processing after the removal of iron, aluminum, and chromium. The inorganic elements found and their respective concentrations in the leach liquor were Ni (3.0 $g.L^{-1}$), Co (0.2 $g.L^{-1}$), Mn (1.2 $g.L^{-1}$), Ca (0.5 $g.L^{-1}$), Mg (7.5 $g.L^{-1}$), Zn (0.08 $g.L^{-1}$) e Cu (0.01 $g.L^{-1}$). After the solvent extraction process, 3% of the manganese ions remained in the refined liquor. Similarly, Crundwell et al.[6] observed that in the industrial purification of nickel, 0.02 $mg.L^{-1}$ of Mn^{2+} ions still remained in the purified solution after the removal of impurities from the leached liquor. Tinkler and Soler[7] indicate that for copper ores, the main impurities that accumulate in the leach solution are Mn and Fe. As iron is removed by solvent extraction, Mn becomes the main impurity in the purified solution, which builds up as the electrolyte solution is recycled during the industrial process. Although the effect of manganese ions is well-known in nickel and copper processing, there is limited research on their impact on cobalt.

Recently, significant investments in the cobalt recovery sector have been intensively implemented to supply the growing demand for this metal, which is a critical element widely used in the production of rechargeable batteries and electric vehicles[3,8,9]. Additionally, the military and aerospace industries are major consumers of metallic cobalt due to its high corrosion resistance[10,11]. This increase in cobalt production has prompted more detailed investigations into the effects of various factors on metallic cobalt production, particularly in electrowinning.

In terms of pure cobalt, the literature includes several articles discussing the consequences of pH variations, current density, temperature, concentration, number of impurities, and specific additives on cobalt electrowinning[2,10,12-16]. However, the impact of impurities on the physical and chemical aspects of metallic cobalt remains unexplored.

Although lead-alloy anodes are widely used for metal electrowinning from acidic sulfate solutions, they exhibit a high overpotential for the oxygen evolution reaction, which

*e-mail: danielle.costal@coppe.ufrj.br

contributes to increased SEC. On the other hand, despite their higher costs, dimensionally stable anodes (DSAs) offer a significant advantage due to their lower overpotential for oxygen evolution, thereby reducing energy consumption. Passos et al.[12] reported that cobalt electrowinning tests using lead anodes yielded a current efficiency of 92.2% ± 0.2% and a SEC of 1.97 kWh.kg^{-1} ± 0.02%. These experiments were conducted in a cobalt sulfate solution containing 60 g.L^{-1} of Co^{2+} ions, at a pH of 4, a temperature of 70°C, and a current density of 200 A.m^{-2}. In contrast, Castro et al.[10] performed similar tests using a Ti/RuO_2 anode under the same conditions, achieving a significantly higher current efficiency of 99.15% ± 0.08% and a lower SEC of 1.60 kWh.kg^{-1} ± 1%. Employing dimensionally stable anodes like Ti/RuO_2, has been shown to enhance the entire effectiveness of the electrowinning by providing higher efficiencies and reduced energy consumption. The MnO_2 deposition on the anode surface can reduce the catalytic activity of such dimensionally stable anodes.

According to Tripathy et al.[17], the total of 10 g.L^{-1} of Mn^{2+} ions in the cobalt electrowinning solution increases current efficiency to 99.9%, while higher concentrations, up to 100 g.L^{-1}, reduce the efficiency to 99.5%. Additionally, Tripathy et al.[17] observed that a fraction of this manganese is oxidized at the anode and that the increase of its concentration favors the oxidation. Churchward et al.[18] reported that nickel has no significant effect on cobalt electrowinning, but manganese, at low concentrations, acts as an anodic depolarizer. Kordesch et al.[19] stated that the existence of Mn^{2+} ion impurities detrimentally influence the quality of cobalt deposition. The formation of a manganese dioxide (MnO_2) layer on dimensionally stable anodes (DSAs), such as those coated with ruthenium oxide (Ti/RuO_2), can lead to a reduction of catalytic activity of such anodes during metal electrowinning processes. The RuO_2 layer is established for its optimum electrical conductivity and high catalytic activity for various electrochemical interactions, including oxygen evolution reactions. However, the deposition of MnO_2 can alter the electron transfer mechanism on the anode surface and increasing the oxygen evolution overpotential. Thus, the influence of Mn^{2+} ions concentration on CE and SEC during cobalt electrowinning with DSA anodes become more critical than with lead-alloys anodes and deserves investigation.

This study investigates the impact of Mn^{2+} ion concentration on CE, SEC, morphology, composition, purity and the physical characteristics of cobalt deposits obtained through electrowinning. Although there is limited literature available on this topic[17-19], this research adopts a comprehensive methodology, utilizing a range of techniques including cyclic and linear voltammetry, electrowinning experiments, scanning electron microscopy (SEM), energy-dispersive X-ray spectroscopy (EDS), optical microscopy, X-ray diffraction (XRD), microhardness testing, and thermogravimetry. These approaches aim to yield consistent and novel insights into the physical and chemical properties of cobalt deposits produced by electrowinning. The investigation covers various aspects, including morphology, hardness, growth structure, and crystalline phases, as well as the sizes of grains and crystallites. Additionally, the study examines the influence of Mn^{2+} ion concentration and its threshold levels on both cathodic and anodic processes. Figure 1 highlights the significance of this research.

2. Materials and Methods

The methodology employed in this study was based on the work of De Castro et al.[10], whose research served as the foundation for the continued development of our experiments and analyses. The controlled variables, equipment used, and experimental conditions—such as temperature, pH, and concentration—were established in accordance with

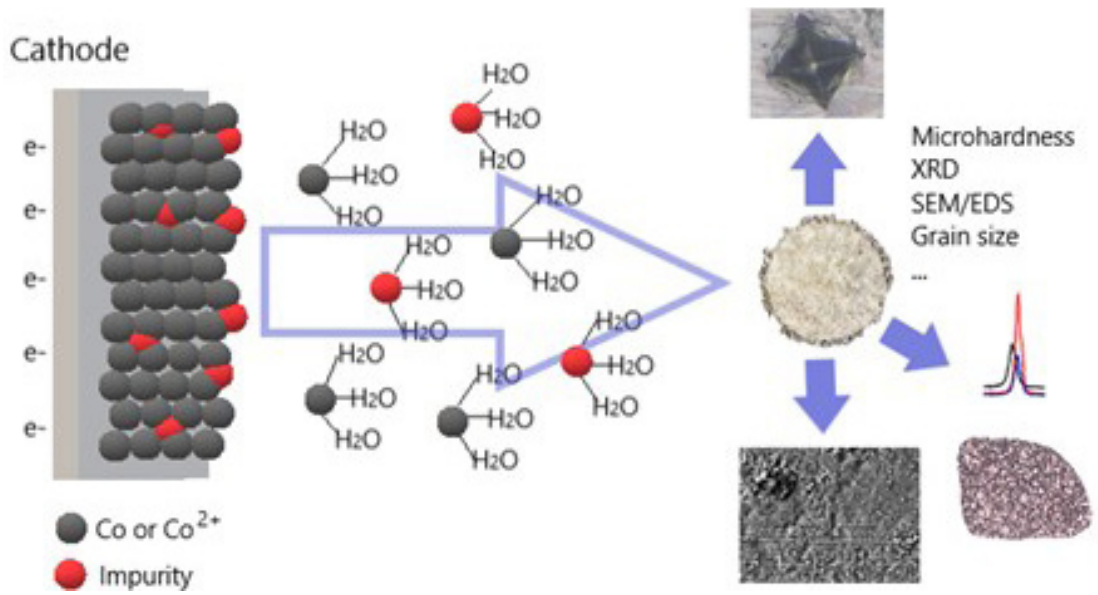

Figure 1. Diagram illustrating the cobalt electrowinning process with the influence of impurities. Impurities significantly compromise the integrity of the cobalt deposits, leading to brittleness. In the schematic, XRD stands for X-ray Diffraction, while SEM/EDS represents Scanning Electron Microscopy and Energy Dispersive Spectroscopy. Gray spheres denote cobalt atoms, and red spheres represent impurity particles.

the guidelines presented in the original study, ensuring the consistency and reproducibility of the results.

2.1. Cyclic and linear voltammetry experiments with cobalt sulfate solutions

During the voltammetry experiments, four distinct high-purity cobalt sulfate solutions were made in 3 L graduated flasks, each with specific concentrations of Mn^{2+} ions added. The prepared solutions were then placed into a 3 L electrochemical cell. Consistent with prior research conducted by Passos et al.[12], the experimental conditions—temperature, pH, and cobalt concentration—were held constant throughout the study. Thus, a cobalt sulfate solution containing 60 $g \cdot L^{-1}$ of Co and a pH of 4 was introduced into a cell maintained at 60°C using a thermostatic bath. Each solution was enriched with Mn^{2+} ions at the concentrations outlined in Table 1.

The voltammetry experiments were conducted with a potentiostat (Metrohm Autolab®) connected to an electrochemical compartment. This cell consisted of a $CoSO_4$ solution and three electrodes: a working electrode made of AISI 304 stainless steel with a contact area of 0.385 cm^2, a counter electrode consisting of a Ti/RuO_2 plate with a surface area of 10 cm^2, positioned 2.5 cm horizontally from the working electrode, and a reference electrode (Ag/AgCl/KCl 3M) located near the working electrode. The scanning speed for the experiments was set at 1 $mV.s^{-1}$. To evaluate cathodic behavior, initial and final potentials of 0.0 V and -0.8 V were applied. For the anodic behavior, the Ti/RuO_2 became the working electrode, and the counter electrode became the stainless steel. The potential was systematically varied between 0.0 V and 3.0 V. The findings were shown as plots of current density ($mA.cm^{-2}$) versus potential (V).

2.2. Cobalt sulfate electrowinning experiments

Electrolytic cobalt deposition tests were conducted in the presence of Mn^{2+} ions using 3 L solutions of cobalt sulfate. The experimental conditions were consistent with those outlined by Passos et al.[12], maintaining a temperature at 60°C, an initial pH of 4, a concentration of 60 $g.L^{-1}$ of Co, and a current density of 200 $A.m^{-2}$. Each electrolyte solution was exposed to a distinct concentration of Mn^{2+} ions, as specified in Table 2. Consequently, four separate experiments were performed, each in triplicate.

The current efficiency of each trial was assessed by dividing the weight of the deposit by the theoretical weight, as calculated using Faraday's law. Additionally, the SEC was computed using Equation (1).

$$SEC = I \cdot t \frac{V}{CE} \quad (1)$$

The V represents the operating voltage, and the result of I multiplied by t corresponds to the charge needed to deposit 1 kg of cobalt, which is equivalent to 909.4 A·h. The weight of the metallic cobalt was assessed using a high-precision balance following a drying process at 120°C.

The cobalt deposits were characterized in terms of morphology and purity through scanning electron microscopy (SEM). The analysis was conducted using a

Table 1. Concentrations interval of Mn^{2+} ions in $CoSO_4$ for voltammetry experiments.

Impurity introduced in the solution of $CoSO_4 \cdot 7H_2O$	Concentrations range ($g.L^{-1}$)
Mn^{2+} ions	0.01 - 0.12

Table 2. Mn^{2+} ions concentrations in $CoSO_4.7H_2O$ solution.

Level	Mn^{2+} ions ($g.L^{-1}$)
Minimum (-)	0.01
Maximum (+)	0.12
Central Point	0.06

TESCAN® VEGA3 instrument, paired with a BRUKER® energy dispersive spectroscopy (EDS) system for detailed compositional insights. To complement the SEM findings, macroscopic images of the deposits were captured using an Avanscope® digital optical microscope, providing a comprehensive view of the deposit structure.

X-ray diffraction (XRD) was employed to identify the crystalline phases of the cobalt deposits, utilizing a Bruker-AXS D8 Endeavor instrument. The analysis was carried out under precise conditions, incorporating Cu Kα radiation with a wavelength (λ) of 0.15406 nm. The generator settings were maintained at 40 kV and 40 mA, while the goniometer was operated at a speed of 0.02°/s. The data was collected across a 2θ range of 4° to 105° with the assistance of a LynxEye position-sensitive detector. For phase identification and quantification, Diffrac.Eva and Diffrac.Topas software were utilized in conjunction with the PDF2+ database. The assessment of crystallographic orientations was performed using spherical harmonic parameters. Additionally, the width at half height of the diffraction peaks was determined from the XRD diffractograms by applying the peak shaping function in Topas software. Crystallite size was calculated according to Equation (2)[20].

$$D = \frac{k\lambda}{\beta cos\theta} \quad (2)$$

In this equation, D represents the crystallite size, k is a shape-dependent constant, λ denotes the wavelength of incidence, β stands for the width of the full width at half maximum (FWHM), and θ indicates the Bragg angle.

To assess the grain size of the deposits, each sample underwent a polishing procedure using 320, 600, and 2500 grit sandpaper, followed by polishing with diamond paste in particle sizes of 6, 3, and 1 micrometer. Subsequently, an acid etching process was performed using a 200 mL aqueous solution composed of 4 grams of picric acid and 4 grams of ferric chloride, which helped reveal the contours of the microstructure.

The microhardness of the cobalt metallic deposits was evaluated using a microhardness tester following the Vickers method, with an applied load of 0.300 kgF, as described in Equation (3)[21].

$$HV = \frac{1{,}854\,P}{d^2} \quad (3)$$

In this equation, HV represents the hardness, d denotes the mean length of the diagonals of the diamond impression, converted to millimeters, and P stands for the load in kgF.

The test samples underwent micrographic analysis, with the captured images processed using ImageJ® software for image analysis[22]. This process enabled the assessment of grain boundaries and their median area within the deposits, facilitating the determination of the average grain size. To guarantee the accuracy and representativeness of the results, a minimum of 50 measurements were taken from one edge of the contour to the opposite edge.

A thermogravimetric study of cobalt deposits was conducted using the LABYS EVO TGA/DTA/DSC 1600 equipment from SETARAM INSTRUMENTATION. The main objective was to quantify the release of gases, such as H_2O and CO_2, resulting from the decomposition of hydroxylated and oxide compounds, possibly associated with impurities. These tests were conducted in an inert nitrogen atmosphere.

3. Results and Discussion

3.1. Influence of Mn^{2+} ions concentration on cyclic and linear voltammetry tests

Figure 2a and Figure 2b illustrate the impact of varying Mn^{2+} ion concentrations on the recorded voltammograms.

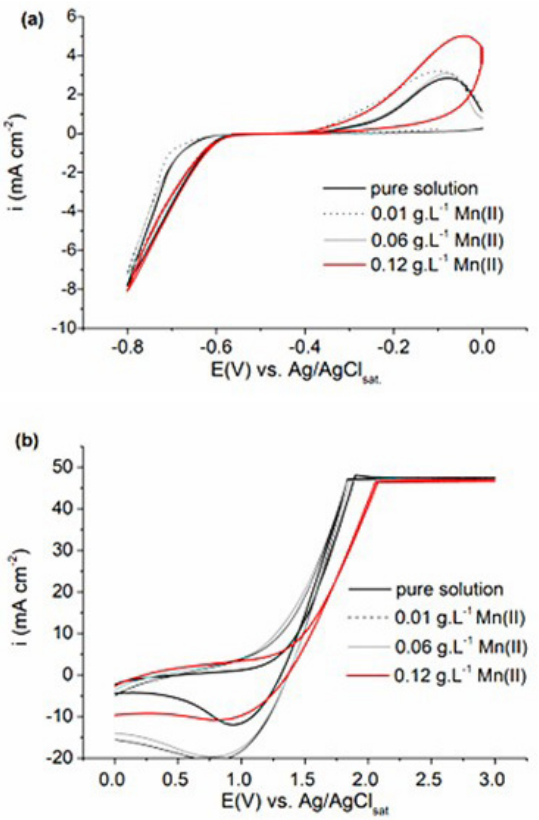

Figure 2. Influence of Mn^{2+} ion concentration on cobalt voltammograms. The $CoSO_4$ solution contains 60 $g \cdot L^{-1}$ of Co^{2+} ions at 60°C, pH 4 and scan rate applied of 1 $mV \cdot s^{-1}$. (a) Displays cathodic cyclic voltammetry (b) Displays anodic linear voltammetry.

Figure 2a illustrates that a higher concentration of Mn^{2+} ions in cobalt sulfate solution caused a slight increase in cathodic current density measured during the cathodic sweep.

Additionally, higher concentrations of this impurity shifted the onset potential for cobalt ion reduction toward less negative responses, favoring the reduction of Co^{2+} ions in the impurity's presence. Furthermore, a small fraction of MnO_2 trapped in the cobalt deposit can be reduced to manganese ions, as described by the reaction in Equation 4.

$$MnO_2 + 4H^+ + 2e^- \rightarrow Mn^{2+} + 2H_2O \; ; \; E^0 = 1.22V \qquad (4)$$

According to Cristiano et al.[23], the surface charge of pyrolusite (MnO_2) is positive, and its point of zero charge occurs in the pH range of 4 to 5. This suggests the possible adsorption of manganese from complexes formed with oxygen on the cathodic deposit. Regarding the impact of Mn^{2+} ions on the anodic behavior during cobalt electrowinning (Figure 2b), an increase in Mn^{2+} ion concentration resulted in a marked rise in anodic polarization. This observation indicates that higher concentrations of Mn^{2+} contribute to greater energy consumption during the process.

3.2. Influence of Mn^{2+} ions concentration on cobalt electrowinning

The effects of Mn^{2+} ion concentration on the physical and chemical properties of metallic cobalt deposits produced by cobalt electrowinning were investigated. Key factors assessed included current efficiency, specific energy consumption, deposit morphology, microhardness, visual appearance, crystallographic orientation, and the grain and crystallite sizes of the cobalt deposits.

3.2.1. Influence of Mn^{2+} ions concentration on CE and SEC

Table 3 presents the results for CE and SEC during cobalt electrowinning in the occurrence of Mn^{2+} ions, including their respective standard deviation values. The relative standard deviation indicates a high degree of reliability in the data's accuracy, remaining below the acceptable analytical limit of 4% relative error. This indicates that the results are consistent and trustworthy for further analysis and interpretation.

The concentration of Mn^{2+} ions in the cobalt electrowinning solution significantly influenced CE. Specifically, the highest concentration tested (0.12 $g \cdot L^{-1}$) achieved the maximum CE, reaching 92.63%. According to Tripathy et al.[17], lower concentrations of Mn^{2+} ions (1 $g.dm^{-3}$) in cobalt sulfate solutions caused an increase in CE (99.8%). However, despite the increase in CE, there is a noticeable rise in the SEC with the presence of Mn^{2+} ions concentration of 0.12 $g.L^{-1}$. At this concentration, the SEC was 1.96 $kWh.kg^{-1}$. This increase can be attached to the growth of a MnO_2 deposit on the anode surface, which decreases the catalytic activity of the DSA anode, as evidenced by the increase in anodic current in the voltammogram (Figure 2b). The highest Mn^{2+} ions concentration (0.12 $g.L^{-1}$) caused the highest SEC(1.96 $kWh.kg^{-1}$). Nevertheless, this SEC value for cobalt electrowinning is considerably lower than those typically achieved with lead

alloy anodes, which range from 1.97 to 2.14 $kWh.kg^{-1}$ with a current efficiency of 200 A m^{-2} , and pH equal to 4 at 60°C[12].

The influence of Mn^{2+} ion concentration on the morphology of cobalt metal deposits were tested through macroscopic observations, which focused on the appearance and structure of the deposits. Figure 3 exhibits the macrographs of cobalt buttons produced at different concentrations of Mn^{2+} ions.

It can be observed that the concentration of Mn^{2+} ions altered the aspect of deposits, especially at the edges. For low concentrations (0.01 $g.L^{-1}$), there is no evident morphology alteration in comparison to those derived from the pure solution; both exhibit uniform morphological characteristics with the formation of smooth and clear deposits. Conversely, for Mn^{2+} ions concentration higher than 0.06 $g.L^{-1}$ there is a preferential cobalt deposition at the cathode edges. As emphasized by Tripathy et al.[17], and Kordesch et al.[19], the increase in manganese ions concentration is detrimental to the quality of cobalt deposits.

3.3. Effect on the chemical and physical characteristics of metallic cobalt deposits

3.3.1. SEM and EDS analyses

The effect of Mn^{2+} ion concentration on the cobalt structure formation is shown in Figure 4. It can be noted that an increase in Mn^{2+} ions concentration promotes non-uniform growth of cobalt grains. Additionally, the formation of holes becomes apparent with higher Mn^{2+} ion concentrations, particularly near the deposit surface close to the metal-solution interface. At an Mn^{2+} ions concentration of 0.12 $g.L^{-1}$, stretch marks are evident. According to Tripathy et al.[17], increased manganese ion concentration degrades the appearance of the deposits: at low concentrations, elongated crystals are observed, while at high concentrations, nodular crystals form.

The components of the cobalt buttons can provide significant facts about the incidence of impurities since Mn^{2+} ions can be adsorbed on deposits associated with hydrogen or oxygen. Figure 5 exhibits an EDS analysis of the metallic cobalt deposits with different concentrations of Mn^{2+} ions to assess the purity of cobalt deposits.

It is noticeable that there is an increase in oxygen concentration near the holes, suggesting the formation of cobalt hydroxides compounds in the deposits. Another factor to be considered is the entrapment of manganese dioxide on the cobalt deposits, followed by its reduction to Mn^{2+} ions, even at low concentrations, which confirms the detrimental influence of Mn^{2+} ions on the deposit quality. As the cathodic potential is not negative enough to permit the reduction of Mn^{2+} to metallic Mn, this is not likely to be

Table 3. Effect of Mn^{2+} ions concentration on CE and SEC for electrowinning tests.

Concentration ($g.L^{-1}$)	CE average (%)	SD (%)	SEC average ($kWh.kg^{-1}$)	SD (%)	Cell potential (V)
Pure solution					
0.00	90.64	1.00	1.80	4.00	1.76
Mn^{2+} ions					
0.01	90.83	0.03	1.86	4.00	1.86
0.06	91.47	2.00	1.85	1.00	1.86
0.12	92.63	0.02	1.96	0.04	2.00

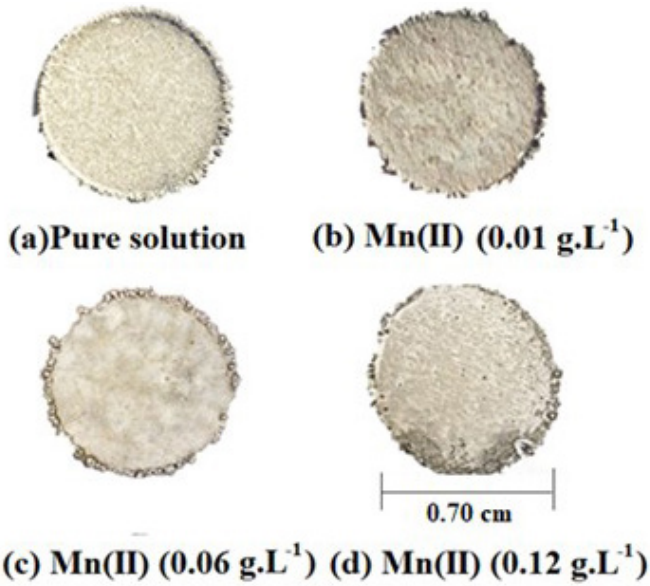

Figure 3. Influence of Mn^{2+} ion concentration on the morphology of cobalt buttons produced through electrowinning in an electrolytic cell containing 3 L of (a) cobalt sulfate pure solution, with a Co^{2+} ion concentration of 60 $g \cdot L^{-1}$, conducted at a temperature of 60°C and a pH of 4; (b) with 0.01 $g.L^{-1}$ of Mn^{2+} ion; (c) with 0.06 $g.L^{-1}$ of Mn^{2+} ion and (d) with 0.12 $g.L^{-1}$ of Mn^{2+} ion.

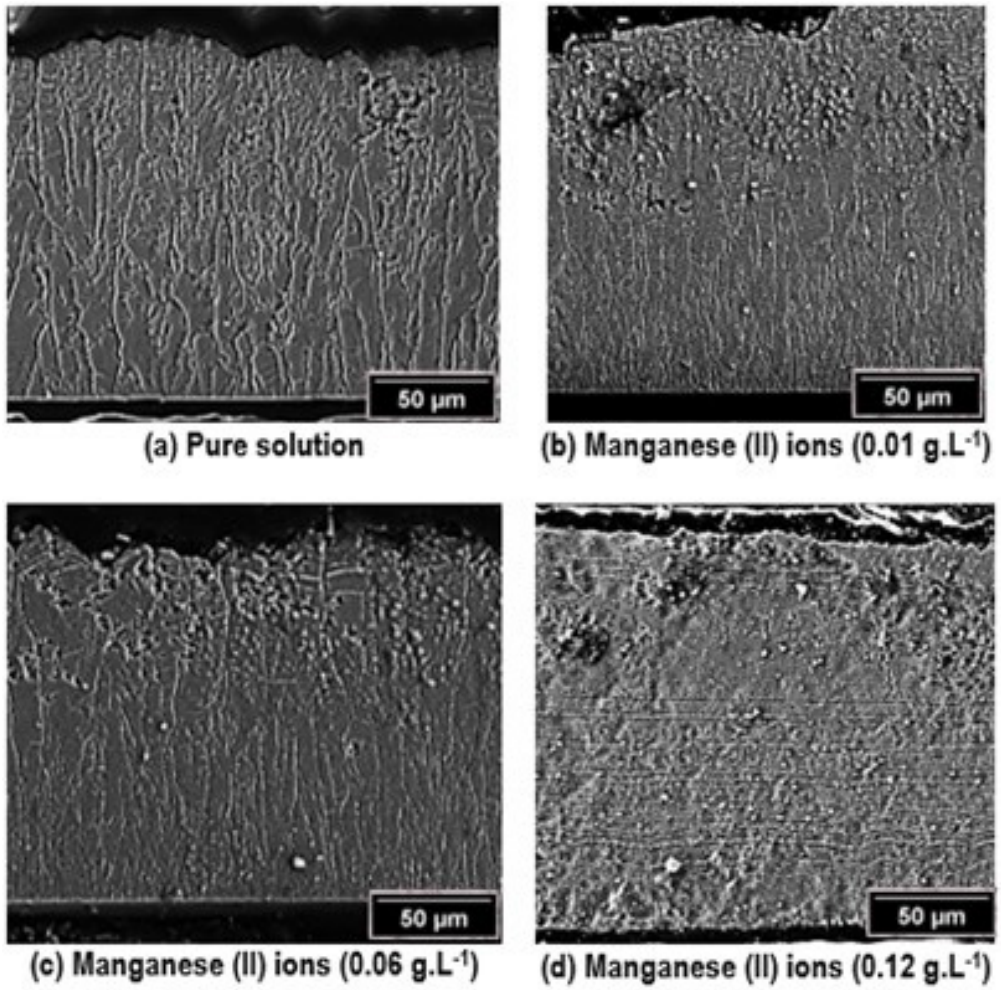

Figure 4. Cross-section images of cobalt deposits obtained through electrowinning from cobalt sulfate solutions with varying concentrations of Mn^{2+} ions are presented. (a) pure solution of cobalt sulfate; (b) with 0.01 g.L^{-1} of Mn^{2+} ion; (c) with 0.06 g.L^{-1} of Mn^{2+} ion and (d) with 0.12 g.L^{-1} of Mn^{2+} ion.

the source of the deposit contamination by Mn. However, it is possible that manganese, in the form of oxide and hydroxide complexes, could migrate to the cathode (as they are positively charge[19] and, consequently, being adsorbed onto the deposit, given that the pH of the initial and final solutions in the cobalt electrowinning process were 4 and 3.5, respectively.

The following equations describe the mechanisms of the reaction for the formation of MnO_2 at the anode, a phenomenon expected in electrodeposition processes in the presence of Mn^{2+} ions in acidic solutions[24].

$$Mn^{2+} \rightarrow Mn^{3+} + e^{-} \; ; \; E^{0} = 1.51V \tag{5}$$

At low acid concentrations, Mn^{3+} can disproportionate or hydrolyze, according to equations (2) and (3)[24].

$$2Mn^{3+} \rightarrow Mn^{2+} + Mn^{4+} \tag{6}$$

$$Mn^{3+} + 2H_2O \rightarrow MnOOH + 3H^{+} \tag{7}$$

The intermediate species MnOOH can be oxidized to produce manganese dioxide[24].

$$MnOOH \rightarrow MnO_2 + H^{+} + e^{-} \tag{8}$$

The reduction of deposited manganese dioxide on the cathode can occur through the following electrochemical steps[24].

$$MnO_2 + H^{+} + e^{-} \rightarrow MnOOH \tag{9}$$

$$MnOOH + 3H^{+} + e^{-} \rightarrow Mn^{2+} + 2H_2O \tag{10}$$

According to Kordesch et al.[19], Mn^{2+} ions also precipitate as MnO_2 at the anode during the electrodeposition process. The MnO_2 layer formed at the anode during electrolysis is likely to detach and get adsorbed onto the cathode during prolonged electrolysis[25]. This behavior is supported by

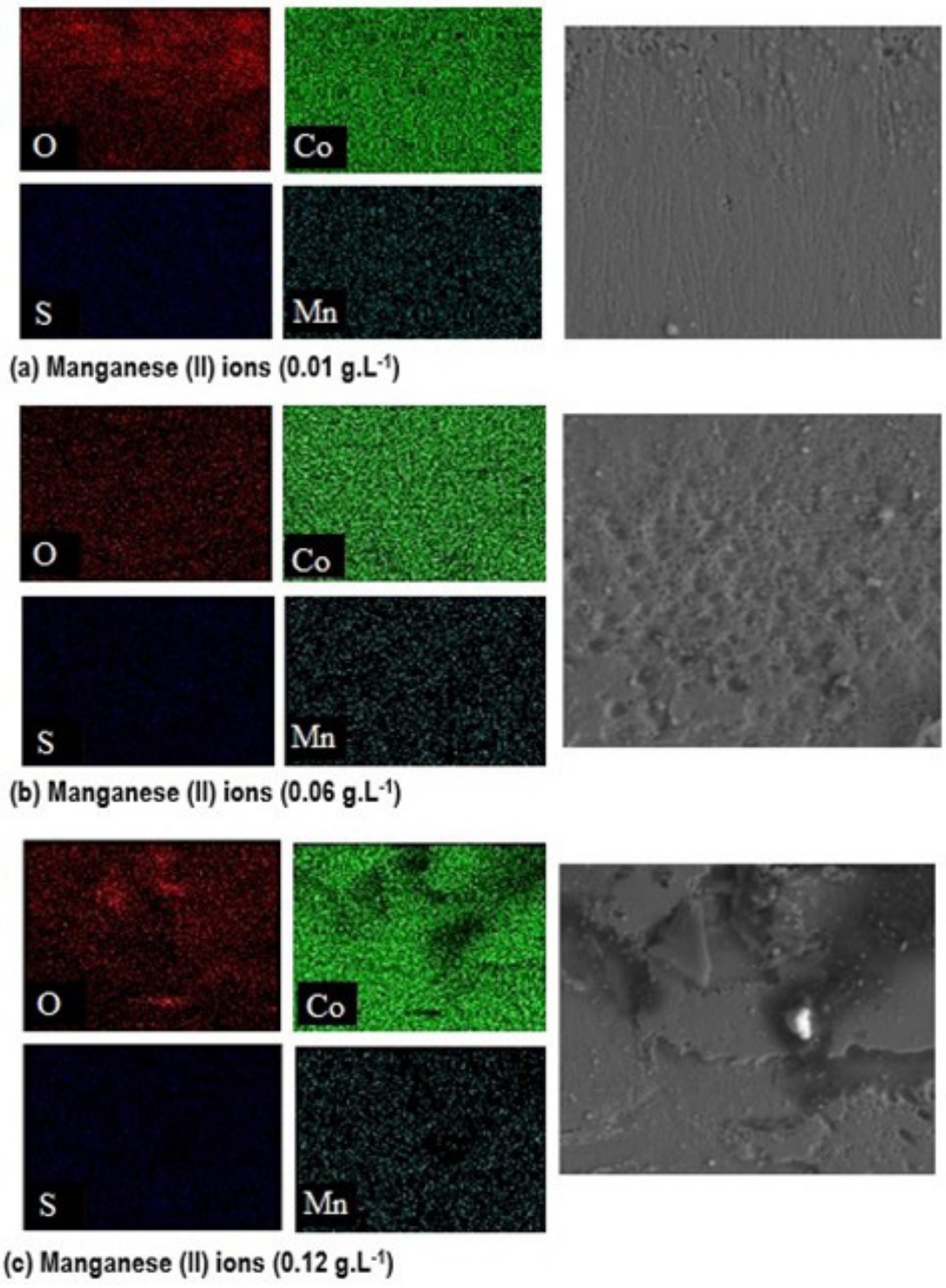

Figure 5. EDS analysis of metallic cobalt buttons in the incidence of different Mn^{2+} ions concentrations. Scale: 40 µm. Focused on oxygen, cobalt, sulfur, and manganese detection. (a) pure solution of cobalt sulfate with 0.01 $g.L^{-1}$ of Mn^{2+} ion; (b) pure solution of cobalt sulfate with 0.06 $g.L^{-1}$ of Mn^{2+} ion and (c) pure solution of cobalt sulfate with 0.12 $g.L^{-1}$ of Mn^{2+} ion.

the fact that the point of zero charge for MnO_2 occurs at approximately pH 4.5, meaning that at pH below 4, the surface charge of MnO_2 is positive[23], thereby being attracted to the cathode due to the electric field.

In an industrial context, during the cobalt electrowinning process, the concentration of Mn^{2+} ions in the electrolyte solution tends to increase due to the continuous recycling flow. This increase in Mn^{2+} ions concentration results in

the formation of manganese hydroxide complexes. As the electrolyte solution undergoes multiple stages of circulation and treatment during recycling, there can be a gradual accumulation of these impurities. Despite the efforts to remove or control these impurities, Mn^{2+} ions can be reintroduced into the solution during the recycling phases.

3.3.2. Cobalt deposits thermogravimetric analysis

The thermogravimetric analysis of cobalt deposits was performed under conditions with and without two varying concentrations of Mn^{2+} ions. The analysis is presented in Figures 6a, 6b, and 6c, respectively. An increase in mass loss was observed in 200°C to 400°C. The highest recorded mass loss (1.26%) was observed in Figure 6c, which corresponds to the cobalt deposit obtained with the highest concentration of Mn^{2+} ions.

According to Nguyen et al.[26] and Donne and Dose[27], the temperature from 25°C to 130°C represents the loss of adsorbed, non-combined water in the sample structure. Additionally, Donne and Dose[27] reported that the broad peak in the range from 120°C to 400°C is of particular attention, as it is related to the elimination of structurally combined water from the deposit, such as protons linked to cation vacancies and Mn^{3+} ions within the initial structure. Furthermore, González et al.[28] observed a mass loss of MnOOH close to 300°C. Nguyen et al.[26] reported that the removal of hydroxylated species associated with cobalt occurs in the 300°C to 400°C range. These results align with the thermogravimetric analyses of cobalt deposits from the pure solution shown in Figures 6a, 6b, and 6c. In Figure 6a, a mass loss of only 0.2% was observed in this temperature range, while Figures 6b and 6c show an increase in mass loss to 1.25% and 1.35%, respectively, in the presence of 0.01 $g.L^{-1}$ and 0.12 $g.L^{-1}$ of Mn^{2+} ions. This suggests that MnOOH was adsorbed, as the only variable involved was the concentration of Mn^{2+} ions.

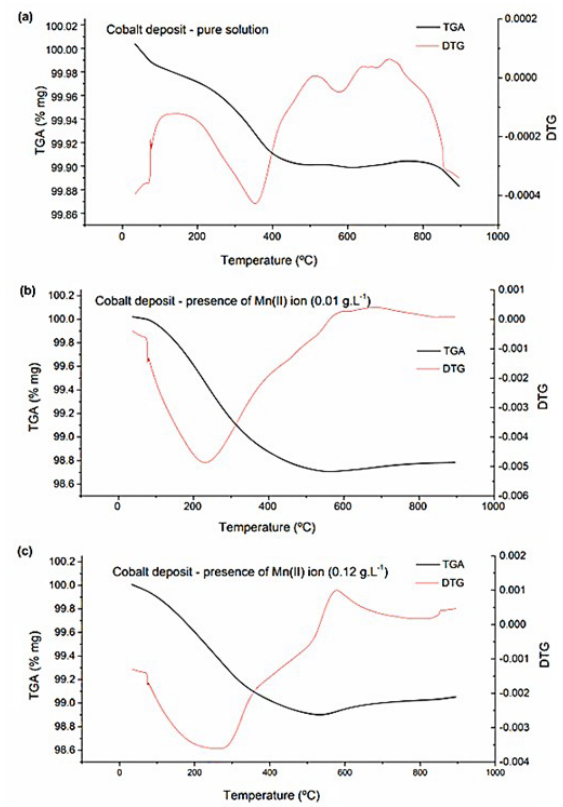

Figure 6. TGA and DTG data for cobalt deposits formed from (a) pure solution, (b) in the presence of 0.01 $g.L^{-1}$ of Mn (II) ions, and (c) 0.12 $g.L^{-1}$ of Mn^{2+} ions.

3.3.3. Distribution of crystalline phases and average dimensions of Co crystallites and grains

The characteristic XRD peaks for cobalt and crystalline phases, obtained by X-ray diffraction, of metallic cobalt deposit obtained by electrowinning in the presence of Mn^{2+} ions concentrations are presented in Table 4, along with their quantification.

As indicated in Table 4, the major crystalline phase of metallic buttons of cobalt is hexagonal close-packed (HCP). Nonetheless, the presence of Mn^{2+} ions resulted in a minor proportion of the face-centered cubic (FCC) crystalline phase. In comparison with deposits formed from the pure solution, the FCC cobalt content decreased from 11% to 6% in the presence of Mn^{2+} ions.

The cobalt diffractograms at varying concentrations of Mn^{2+} ions are showed in Figure 7. The presence of Mn^{2+} ions altered the intensity of the cobalt diffraction peaks in comparison to those obtained from pure solutions. In experiments conducted without impurities, a preferred orientation was noted for the two planes with a peak at 44.3° (002 - HCP and 111 - FCC). In the presence of Mn^{2+} ions at lower concentrations, the preferred orientation was also observed at the peak corresponding to 44.3° (002 - HCP and 111 - FCC). At higher Mn^{2+} ions concentrations, the preferred orientation shifted to peaks at 47-50° (101 - HCP and 200 - FCC) and 41.6° (HCP - 100). Additionally, an increase in the cobalt diffraction peak intensity at 41.6° was observed with the increase in Mn^{2+} ions concentration. Conversely, increasing the concentration of Mn^{2+} ions resulted in a reduction of the cobalt diffraction peak intensity at 44.3°, yielding a profile similar to that observed between 47° and 54°. Therefore, the increase of Mn^{2+} ions concentration increased residual

Table 4. Impact of Mn^{2+} ion concentrations on the crystallographic orientation and phases of metallic cobalt buttons.

	Concentrations ($g.L^{-1}$)	Crystallographic orientation	Crystalline phases (%)
Pure solution	No impurity	(100) (002) (101)	HCP (89%) FCC (11%)
Manganese (II) ions	0.01	(100) (002) (101)	HCP (94%) FCC (6%)
	0.06	(100) (002) (101)	HCP (93.7%) FCC
	0.12	(100) (002) (101)	(6.3%) HCP (94%) FCC (6%)

deformations of the deposits. This increase is indicative of non-uniform residual deformations[29]. Additionally, the occurrence of impurities led to a rightward shift of all cobalt peaks compared to standard deposits, indicating uniform compressive deformations[30].

Apart from examining crystalline phases, the average size of crystallites and grains were also obtained. Figure 8 illustrates the impact of varying concentration of Mn^{2+} ions on the size of cobalt crystallites and grains.

Regarding the average size of cobalt crystallites, an increase of crystallite sizes up to 36 nm can be noted in the presence of Mn^{2+} ions concentration up to 0.06 $g.L^{-1}$. The presence of manganese decreased the nucleation rate and increased the growth rate of crystallites. However, with 0.12 $g.L^{-1}$ of Mn^{2+} ions, there is a decrease in the average crystallite size to approximately 28 nm. Higher manganese concentrations introduce more defects and strain within the crystal structure, leading to a breakup of larger crystallites into smaller ones. In relation to the average grain size results, the average grain size increases with the rising concentration of Mn^{2+} ions, reaching 32 micrometers. As the concentration of Mn^{2+} increases, the growth of larger grains occurs due to reduced boundary energy, and the mobility of individual crystallites within those grains can be hindered, resulting in smaller crystallites. Furthermore, micrographs of the deposits are presented in Figure 9 to verify the Co average grain size in the absence and presence of impurity. In this context, these findings suggest a growth trend for grains, with the presence of this impurity.

Most of the literature addressing the impact of Mn^{2+} ions on the microstructure of alloys and superalloys presents results obtained with significant concentrations of Mn^{2+} ions, typically ranging from 1% to 20% by weight in the alloy composition[31,32]. In this context, the presence of manganese in certain types of alloys and superalloys (such as Ni-Co) promotes grain size reduction, leading to an increase in microhardness[31,32]. In contrast, the manganese ions concentration used in the present research is minimal and directly affects the microstructure of cobalt deposits. The literature lacks information on the impact of Mn^{2+} ions under the specific conditions set forth in this study.

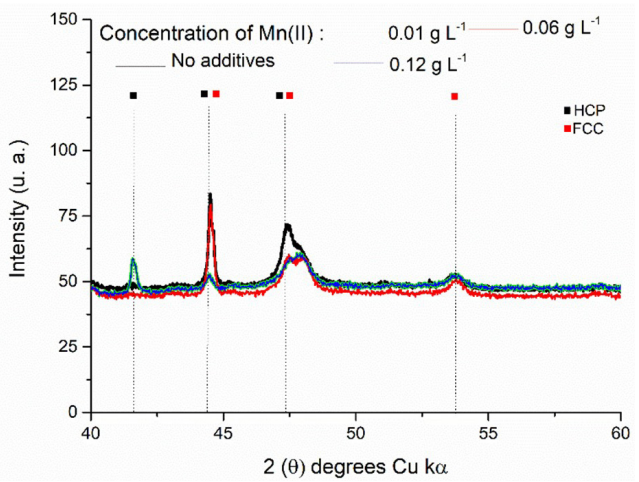

Figure 7. Influence of Mn^{2+} ions concentrations on the orientation of cobalt crystallographic phases.

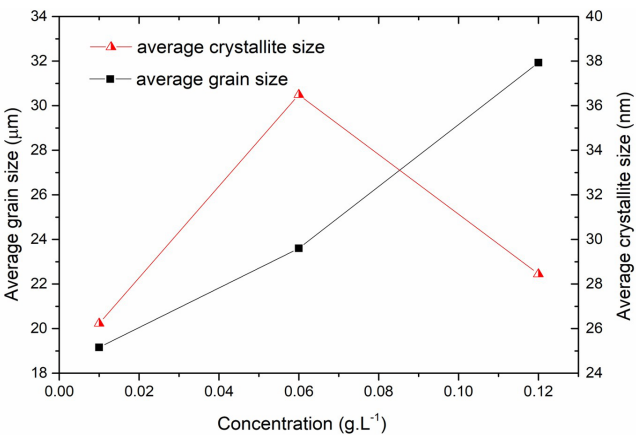

Figure 8. Influence of Mn^{2+} ions concentrations on the average size of cobalt crystallites and grains.

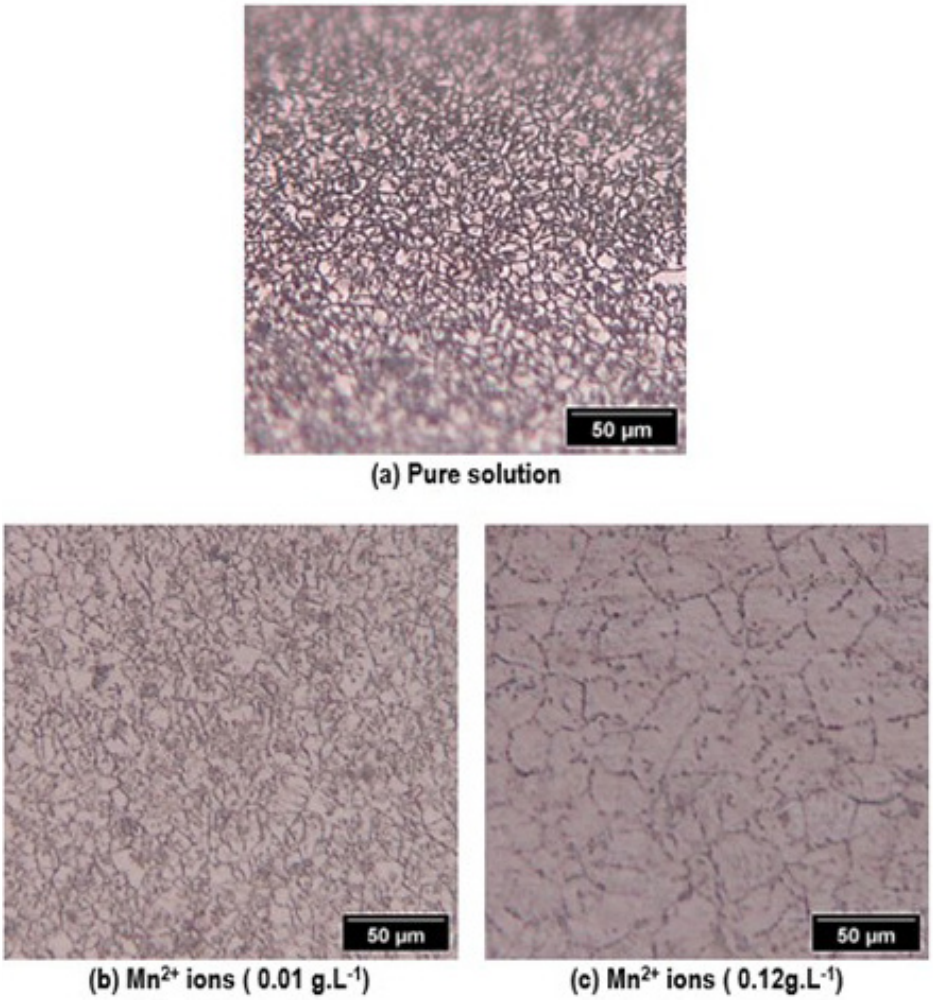

Figure 9. Influence of Mn^{2+} ions concentration on the average size of cobalt grains.

Table 5. Influence of Mn^{2+} ions concentrations on microhardness of metallic cobalt from an electrolyte solution of $CoSO_4.7H_2O$.

Cobalt deposits average size obtained by pure solution: 359 HV		
Mn^{2+} ions concentrations ($g.L^{-1}$)		
0.01	0.06	0.12
Microhardness (HV)		
323	303	292

3.3.4. Microhardness measurements of metallic cobalt obtained by electrowinning

Table 5 presents the impact of Mn^{2+} ion concentration on the microhardness of metallic cobalt deposits. Deposits obtained with Mn^{2+} ion concentrations exceeding 0.01 $g{\cdot}L^{-1}$ demonstrated lower microhardness values compared to those produced from pure solutions. For instance, as illustrated in Table 5, the deposit with 0.12 $g{\cdot}L^{-1}$ of Mn^{2+} ions showed a microhardness of 292 HV, while the microhardness from the pure solution was 359 HV.

The evaluation of microhardness results concerning the presence of impurities supported the observed values for the average sizes of cobalt crystallites and grains. An increase in Mn^{2+} ion concentration led to a decrease in microhardness and an increase in the average sizes of both cobalt crystallites and grains.

4. Conclusions

The effect of Mn^{2+} ion concentration on cobalt cyclic voltammetry indicated that higher concentrations led to a slight increase in cathodic current density measurements recorded during the cathodic scan and shifted the onset potential for cobalt ion reduction to less negative values. Conversely, anodic voltammetry results implied that higher concentrations of Mn^{2+} ions led to a significant increase in polarization. During electrowinning tests, increasing the Mn^{2+} ions concentration led to an improvement in CE. SEC and cell potential were also elevated with a presence of Mn^{2+} ions for DSA. The highest concentration of Mn^{2+} ions resulted in a current efficiency of 92.63%, with specific energy consumption and cell potential reaching 1.96 kWh/kg and 2.00 V, respectively.

Macroscopic images of cobalt deposits demonstrated that manganese's presence deteriorates the appearance of

deposits. For concentrations of Mn^{2+} ions up to 0.06 $g.L^{-1}$, there is a preferential deposition of cobalt deposits at the edges, indicating that manganese increases the charge at those regions.

SEM cross-section images of the deposits revealed notable structural differences. An increase in Mn^{2+} ion concentration resulted in non-uniform growth of cobalt grains, with the highest concentration leading to deposits characterized by stretch marks. EDS analysis showed an accumulation of oxygen around the non-uniformities, along with the presence of manganese. In terms of thermogravimetric results, the highest mass loss observed was 1.35% within the temperature range of 200-400 °C, attributed to the highest concentration of Mn^{2+} ions.

X-ray diffraction results revealed that the prevalent crystalline phase was hexagonal close-packed (HCP). The average crystallite size exhibited a similar pattern to the grain size up to a concentration of 0.06 $g{\cdot}L^{-1}$, where both increased with the presence of Mn^{2+} ions. However, while the grains continued to increase with the higher concentration of Mn^{2+} ions, the crystallite size presented a slight decrease under these conditions, since higher manganese concentrations probably cause more defects in the crystal structure. The varying intensities of the cobalt deposit diffraction peaks, both with and without Mn^{2+} ions, indicated residual deformation. The deposit produced with the highest Mn^{2+} ion concentration had the lowest hardness, measured at 292 HV. In contrast, the deposit formed from the pure solution exhibited a hardness of 359 HV.

Considering all the factors and variables involved in the process the concentration of Mn^{2+} ions should be kept low in order to decrease SEC and to improve deposit quality.

5. Acknowledgments

The authors gratefully acknowledge the support of Instituto Tecnológico Vale (ITV) and the Brazilian agency Coordenação de Aperfeiçoamento de Pessoal de Nível Superior (CAPES). Furthermore, this research was partially funded by CAPES under Finance Code 001.

6. References

1. Slack JF, Kimball BE, Shedd KB. Cobalt: professional paper. Reston: U.S. Geological Survey; 2017. http://doi.org/10.3133/pp1802F.
2. Huang JH, Kargl-Simard C, Alfantazi AM. Electrowinning of cobalt from a sulfate-chloride solution. Can Metall Q. 2004;43(2):163-72. http://doi.org/10.1179/cmq.2004.43.2.163.
3. Zhang T, Bai Y, Shen X, Zhai Y, Ji C, Ma X, et al. Cradle-to-gate life cycle assessment of cobalt sulfate production derived from a nickel-copper–cobalt mine in China. Int J Life Cycle Assess. 2021;26(6):1198-210. http://doi.org/10.1007/s11367-021-01925-x.
4. Cobalt Institute. Cobalt Market Report 2021 [Internet]. 2021 [cited 2023 Mar 20]. Available from: https://www.cobaltinstitute.org/resource/state-of-the-cobalt-market-report-2021.
5. Guimarães AS, Resende GPS, Santos ID, Mansur MB. Selective solvent extraction of nickel and cobalt from a Ni lateritic sulfuric solution using synergism caused by LIX860N-IC and Versatic. Separ Purif Tech. 2024;332:125757. http://doi.org/10.1016/j.seppur.2023.125757.
6. Crundwell FK, Du Preez NB, Knights BDH. Production of cobalt from copper-cobalt ores on the African Copperbelt–An overview. Miner Eng. 2020;156:106450. http://doi.org/10.1016/j.mineng.2020.106450.
7. Tinkler OS, Sole KC. Copper solvent extraction on the African Copperbelt: from historic origins to world-leading status. J South Afr Inst Min Metall. 2023;123(7):349-56. http://doi.org/10.17159/2411-9717/2906/2023.
8. Li M, Lu J. Cobalt in lithium-ion batteries. Science. 2020;367(6481):979-80. http://doi.org/10.1126/science.aba9168.
9. Alves Dias P, Blagoeva D, Pavel C, Arvanitidis N. Cobalt: demand-supply balances in the transition to electric mobility. Luxembourg: Publications Office of the European Union; 2018. http://doi.org/10.2760/97710.
10. Castro DC, dos Santos ID, Neumann R, Ribeiro PPM, Dutra AJB. Effect of additives and Cl^- ions on the physical and chemical properties of cobalt deposits obtained by electrowinning. Metall Mater Trans, B, Process Metall Mater Proc Sci. 2024;55(4):2362-77. http://doi.org/10.1007/s11663-024-03098-y.
11. Hao H, Sun X, Liu Z, Zhao F, Song J. Tracing global cobalt flow: 1995–2015. Resour Conserv Recycling. 2019;149:45-55. http://doi.org/10.1016/j.resconrec.2019.05.009.
12. Passos FACM, Souza JCT, Santos ID, Neumann R, Ribeiro PPM, Dutra AJB. Effect of pH and current density on the physical properties of cobalt obtained by electrowinning from sulfate solutions. Miner Eng. 2024;211:108697. http://doi.org/10.1016/j.mineng.2024.108697.
13. Lu J, Dreisinger D, Glück T. Cobalt electrowinning: a systematic investigation for high-quality electrolytic cobalt production. Hydrometallurgy. 2018;178:19-29. http://doi.org/10.1016/j.hydromet.2018.04.002.
14. Zhou J, Wang S, Song XT. Electrodeposition of cobalt in double-membrane three-compartment electrolytic reactor. Trans Nonferrous Met Soc China. 2016;26(6):1706-13. http://doi.org/10.1016/S1003-6326(16)64279-6.
15. Lupi C, Pilone D. Electrodeposition of nickel-cobalt alloys: the effect of process parameters on energy consumption. Miner Eng. 2001;14(11):1403-10. http://doi.org/10.1016/S0892-6875(01)00154-6.
16. Elsherief AE. Effects of cobalt, temperature and certain impurities upon cobalt electrowinning from sulfate solutions. J Appl Electrochem. 2003;33(1):43-9. http://doi.org/10.1023/A:1022938824111.
17. Tripathy BC, Singh P, Muir DM. Effect of manganese(II) and boric acid on the electrowinning of cobalt from acidic sulfate solutions. Metall Mater Trans, B, Process Metall Mater Proc Sci. 2001;32(3):395-9. http://doi.org/10.1007/s11663-001-0023-9.
18. Churchward RE, Shelton FK, Knickerbocker RG. A study of impurities in cobalt electrowinning. Trans Electrochem Soc. 1944;85(1):193. http://doi.org/10.1149/1.3071593.
19. Kordesch K. Primary batteries—alkaline manganese dioxide-zinc batteries. In: Bockris JO, Conway BE, Yeager E, White RE, editors. Comprehensive treatise of electrochemistry. Boston: Springer; 1981. p. 219-32. https://doi.org/10.1007/978-1-4615-6687-8_6.
20. Cullity BD, Stock SR. Elements of X-ray diffraction. 3rd ed. Upper Saddle River: Prentice Hall; 2001.
21. Fischer-Cripps AC. Measurement of hardness of very hard materials. In: Tiwari A, ed. Solid Mechanics and Its Applications. Dordrecht: Springer; 2014. p. 53-62. http://doi.org/10.1007/978-94-007-6919-9_3
22. Schneider CA, Rasband WS, Eliceiri KW. NIH Image to ImageJ: 25 years of image analysis. Nat Methods. 2012;9(7):671-5. http://doi.org/10.1038/nmeth.2089.
23. Cristiano E, Hu YJ, Sigfried M, Kaplan D, Nitsche H. A comparison of point of zero charge measurement methodology. Clays Clay Miner. 2011;59(2):107-15. http://doi.org/10.1346/CCMN.2011.0590201.
24. Nijjer S, Thonstad J, Haarberg GM. Oxidation of manganese(II) and reduction of manganese dioxide in sulphuric acid.

Electrochim Acta. 2000;46(2-3):395-9. http://doi.org/10.1016/S0013-4686(00)00597-1.

25. Clancy M, Bettles CJ, Stuart A, Birbilis N. The influence of alloying elements on the electrochemistry of lead anodes for electrowinning of metals: A review. Hydrometallurgy. 2013;131-132:144-57. http://doi.org/10.1016/j.hydromet.2012.11.001.
26. Nguyen VM, Konyukhov YV, Ryzhonkov DI. Influence of a rotary electromagnetic field and mechanical stimulation on the production of cobalt nanopowder by reduction with hydrogen. Steel Transl. 2018;48(2):73-7. http://doi.org/10.3103/S0967091218020109.
27. Donne SW, Dose WM. Manganese dioxide structural effects on its thermal decomposition. Mater Sci Eng B. 2011;176(15):1169-77. http://doi.org/10.1016/j.mseb.2011.06.007.
28. González C, Gutiérrez JL, González-Velasco JR, Cid A, Arranz A, Arranz JE. Transformations of manganese oxides under different thermal conditions. J Therm Anal. 1996;47(1):93-102. http://doi.org/10.1007/BF01982689.
29. Boumaiza A, Bouras M, Rouag VJ. XRD peak broadening characterization of deformed microstructures and heterogeneous behavior of carbon steel. Theor Appl Fract Mech. 2012;61:51-6. http://doi.org/10.1016/j.tafmec.2012.08.006.
30. Noyan IC, Cohen JB. Residual stress: measurement by diffraction and interpretation. New York: Springer Verlag; 1987. http://doi.org/10.1007/978-1-4613-9570-6.
31. Park YJ, Kim JW, Hwang MJ, Han MK, Kim YG, Song HJ. Effect of manganese on the microstructure, mechanical properties and corrosion behavior of titanium alloys. Mater Chem Phys. 2016;180:341-8. http://doi.org/10.1016/j.matchemphys.2016.06.016.
32. Srivastava M, Grips VKW, Rajam KS. Influence of cobalt on manganese incorporation in Ni–Co coatings. J Appl Electrochem. 2010;40(4):777-82. http://doi.org/10.1007/s10800-009-0056-3.